Inorganica Chimica Acta 526 (2021) 120515

Contents lists available at ScienceDirect

Inorganica Chimica Acta

journal homepage: www.elsevier.com/locate/ica

Synthesis, characterization and antimicrobial activity of nickel(II) complexes of tridentate N3 ligands

Athulya Das [a], Anjana Rajeev [a], Sarmistha Bhunia [b], Manivel Arunkumar [c], Nithya Chari [c], Muniyandi Sankaralingam [a,*]

[a] Bioinspired & Biomimetic Inorganic Chemistry Lab, Department of Chemistry, National Institute of Technology Calicut, Kozhikode 673601, Kerala, India
[b] School of Chemical Sciences, Indian Association for the Cultivation of Science, Kolkata 700032, India
[c] Department of Microbiology, School of Life Sciences, Bharathidasan University, Tiruchirappalli 620024, Tamil Nadu, India

ARTICLE INFO

Dedicated to Professor Dr. Mallayan Palaniandavar on the occasion of his 70th birthday.

Keywords:
Medicinal inorganic chemistry
Nickel(II) complexes
Heterocyclic compounds
Spectroscopy
Antimicrobial agents

ABSTRACT

The desire to develop new antimicrobial agents against the rising threat of extensive antibiotic resistance led to the exploration of many natural and synthetic compounds. Herein, we report the isolation and structural characterization of nickel(II) complexes of the type $[Ni(L)_2]^{2+}$ (**1** and **2**) of tridentate N3 ligands such as bis(pyridin-2-ylmethyl)amine (L1) and 1-(1-methyl-1*H*-imidazol-2-yl)-*N*-(pyridin-2-ylmethyl)methanamine (L2). Both the complex cations of $[Ni(L1)_2]^{2+}$ (**1**) and $[Ni(L2)_2]^{2+}$ (**2**) possess a distorted octahedral coordination geometry in which Ni(II) is chelated to two equivalents of the tridentate L1 and L2 ligand in facial coordination, respectively. Complexes **1** and **2** exhibit the bands in the visible region in UV–Vis spectra and peaks in the downfield region in paramagnetic NMR spectra suggesting the octahedral coordination geometry of the complexes in solution as well. Further, complexes **1** and **2** were evaluated for their antimicrobial activity against various clinical pathogens. With *in vitro* studies, complex **1** displayed activity against *Vibrio parahaemolyticus* and *V. alginolyticus*, *Staphylococcus aureus*, *Candida albicans*, and *Salmonella typhi,* and complex **2** displayed activity against *S. aureus*, *S. typhi*, and *C. albicans*. In addition, with *in vivo* studies, complex **1** was effective in inhibiting *Vibrio* infection in brine shrimp larvae while having no toxicity on the larvae. We believe these results will encourage medicinal chemists to further the study on metal complexes against multi-resistant pathogens.

1. Introduction

High mortality rate by pathogenic diseases due to antimicrobial resistance (AMR) has become a grave threat for human health and economic development, and AMR has been included in the top 10 global public health threats to humanity by World Health Organization (WHO) [1,2]. Microbes develop AMR through random mutation of the genome and accepting antimicrobial-resistant genes from other microbes. These strains develop ability to reduce or eliminate the effect of antimicrobial agents [3]. To spread the seriousness of AMR, WHO has updated the slogan for a global public awareness campaign, World Antimicrobial Awareness Week (WAAW), as "Antimicrobials: Handle with Care" in 2020 [2]. "Superbugs" formed as a result of AMR, will rule the world within no time if more promising antimicrobial agents are not discovered [4]. Medicinal chemists are poised to play a central role in addressing the key scientific challenges toward the development of metal-based antimicrobial agents. Especially, earth-abundant transition metal complexes play a major role in biological functions (enzymes) and their potential against various diseases have inspired bioinorganic chemists to explore transition metal complexes for improved pharmacological activities [5–9]. A huge amount of antimicrobial data reveals that the activity of the ligand is enhanced when it is chelated with metal ion [10–12]. Further, a possible mode of increased activity of metal chelates can be explained on the basis of Overtone's concept and Tweedy's chelation theory [13]. In addition, chelation could enhance the lipophilic character of the central metal to favour its permeation through lipid bilayers of the cell membrane and that results in an increased uptake of the metal chelates [14].

Among the transition metal complexes, the significance of nickel in bioinorganic chemistry has rapidly increased after the discovery of the nickel enzyme, urease [15,16]. Following to this, a number of nickel complexes have been reported with a broad-spectrum of activity against pathogens, which is expected due to the ability of such complexes can penetrate into the microbial cells and affect the enzyme activity

* Corresponding author.
E-mail address: msankaralingam@nitc.ac.in (M. Sankaralingam).

https://doi.org/10.1016/j.ica.2021.120515
Received 20 February 2021; Received in revised form 6 June 2021; Accepted 11 June 2021
Available online 17 July 2021

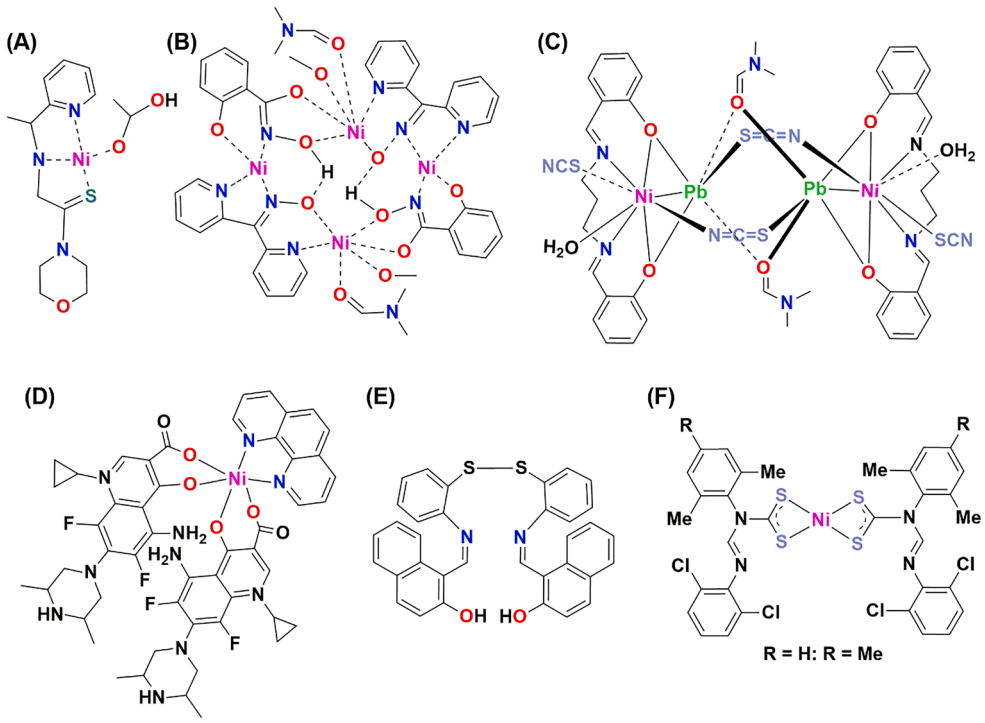

Scheme 1. Reported nickel complexes and ligand (**E**) having antimicrobial activity [17–23].

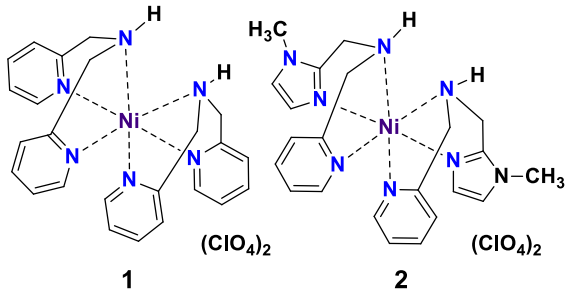

Scheme 2. Nickel(II) complexes used in this study.

[17–23]. For example, in 2001, Nomiya *et al* reported a series of nickel complexes with thiosemicarbazone and semicarbazone ligands for antimicrobial studies. Among them complex **A** in Scheme 1 showed selective and effective activity against *Bacillus subtilis* and *S. aureus* (Gram-positive) with a minimum inhibitory concentration (MIC) of 31.3 μg/mL [17,18]. Later in 2003, Kessissoglou *et al* studied the relationship between nuclearity and antimicrobial activity using the mixed ligand nickel complexes with salicylhydroxamic acid and di-2-pyridyl-ketonoxime, and among their complexes, **B** in Scheme 1 showed activity against *B. subtilis* with a MIC of 12 μg/mL [19]. Kurtaran *et al* in 2005 reported a heteronuclear nickel complex of *N,N'*-bis(salicylidene)-1,3-diaminopropane, (**C** in Scheme 1), which showed activity against *Enterobacter aerogenes* with a MIC of 31.25 μg/mL [20]. Psomas *et al* reported a series of mixed ligand nickel complexes with diimines and 3rd generation quinolone antibacterial agent sparfloxacin, (**D** in Scheme 1) against *E. coli*, *P aeruginosa*, and *S. aureus*, for which MIC range between 16 - 128 μg/mL [21]. Recently, Singh *et al* reported nickel complexes based on imine donors and observed reasonable MIC between 15 - 31 μg/mL towards *S. aureus*, which is comparable to the standard drug ciprofloxacin (**E** in Scheme 1) [22]. Very recently, Omondi *et al* reported several nickel(II) complexes of formamidine-based dithiocarbamate ligands (**F** in Scheme 1), in which the complexes containing electron-withdrawing substituents showed antimicrobial activity against both Gram-positive and Gram-negative bacteria except for MRSA with MIC ranging between 0.025 - 1000 μg/mL [23]. Thus, there is still much to be investigated in this area to understand the mechanism of action of these nickel complexes by tuning the ligand systems.

More importantly, the ligand system should be tuned with heterocyclic compounds, because more than 90% of the drugs contain heterocycles in which a wide range of them contain five or six-membered nitrogen-containing imidazole and pyridine framework [24–37]. Hence, the present work has been designed to explore pyridyl and imidazolyl nitrogen-containing nickel(II) complexes (Scheme 2) as potential antimicrobial agents. These complexes have been characterized by various spectroscopic techniques and tested for their antimicrobial activity against human and aquaculture pathogens. Therefore, this work is intended to highlight the potential of nickel complexes as antimicrobial agents.

2. Experimental

2.1. Materials

All chemicals were purchased from commercial sources as reagent grade and used directly without further purification unless otherwise specified. Nickel(II) perchlorate hexahydrate, pyridine-2-carboxaldehyde and sodium sulfate were purchased from Avra. Sodium borohydride and 2-picolylamine was purchased from Alfa Aesar and 1-methylimidazole-2-carboxaldehyde was purchased from TCI, and were used as such. Methanol was purchased from Qualigens and acetonitrile from Fischer and both were distilled over calcium hydride before use.

2.2. Physical measurements

The electronic spectra of the complexes were recorded using Agilent Cary 8454 UV–Visible diode array spectrophotometer, using distilled acetonitrile as the solvent at 298 K. The ATR-FTIR spectra of the ligands and complexes were recorded using JASCO 4700, in 4000 to 400 cm^{-1} range. The ^{1}H NMR spectra of the complexes were recorded using Bruker

400 MHz, using deuterated acetonitrile as the solvent and tetramethylsilane as the internal reference. The mass data of the complexes were recorded using Waters QTOF Micro YA263. The crystal structure of complex **2** was determined by carrying out the diffraction experiments using the Bruker SMART APEX diffractometer. The TGA and DSC analysis were carried out on a TGA Q50 thermal analyser.

2.3. Synthesis of ligands

The present ligands L1 and L2 have been synthesized according to the literature methods [38–42].

2.3.1. Bis(pyridin-2-ylmethyl)amine (L1)

Yield 0.993 g (99.6%). ^{1}H NMR (400 MHz, CD_3CN) (ppm) (Fig. S1A): 5.45 (s, 1H), 7.2–8.6 (m, 4H), 3.95 (s, 4H). IR data (ATR, cm^{-1}) (Fig. S2A): 3336 ν(NH), 745 ν(CN).

2.3.2. 1-(1-methyl-1H-imidazol-2-yl)-N-(pyridin-2-ylmethyl)methanamine (L2)

Yield 0.583 g (63.6 %). ^{1}H NMR (400 MHz, CD_3CN) (ppm): (Fig. S1B) 5.45 (s, 1H), 7.2–8.6 (m, 4H), 3.63 (s, 3H), 3.85 (s, 2H), 3.81 (s, 2H). IR data (ATR, cm^{-1}) (Fig. 2): 3347 ν(NH), 752 ν(CN).

2.4. Isolation of the nickel(II) complexes

The present complexes **1** and **2** have been isolated according to the literature methods [39].

$Ni(ClO_4)_2{\cdot}6H_2O$ (91 mg, 0.25 mmol) was stirred and dissolved in 1 mL of methanol and to this, a methanolic solution (1 mL) of ligand (0.5 mmol) was added dropwise with constant stirring. After 1 h, the pink precipitate formed was filtered through a G4 crucible, washed with cold methanol and diethylether. The pink precipitate was dried under a vacuum.

2.4.1. $[Ni(L1)_2](ClO_4)_2$ (1). Complex 1 was prepared using the above general procedure using L1

Yield 90%. TOF MS *m/z* (Fig. S3): 228.09 $[Ni(L1)_2]^{2+}$, 256.05 $[Ni(L1)]^+$, 356.01 $\{[Ni(L1)](ClO_4)\}^+$, 555.14 $\{[Ni(L1)_2](ClO_4)\}^+$, 200.13 $(L1H)^+$. IR data (ATR, cm^{-1}) (Fig. S2B): 3282 ν(NH), 753 ν(CN), 1052, 911 $\nu(ClO_4^-)$. UV–Vis. λ_{max} (nm) (ε, in M^{-1} cm^{-1}) in CH_3CN (Fig. 1): 801 (10), 511 (7), Elemental analysis calcd (%) for; $C_{24}H_{26}N_6Cl_2O_8Ni$: C 43.94, H 3.99, N 12.81; found: C 43.84, H 3.89, N 12.84.

2.4.2. $[Ni(L2)_2](ClO_4)_2$ (2): Complex 2 was prepared using the above general procedure using L2

Yield 35.8%. TOF MS *m/z* (Fig. S4): 231.11 $[Ni(L2)_2]^{2+}$, 259.07 $[Ni(L2)]^+$, 561.19 $\{[Ni(L2)_2](ClO_4)\}^+$, 203.15 $(L2H)^+$. IR data (ATR, cm^{-1}) (Fig. 2): 3304 ν(NH), 760 ν(CN), 1062, 901 $\nu(ClO_4^-)$. UV–Vis. λ_{max} (nm) (ε, in M^{-1} cm^{-1}) in CH_3CN (Fig. 1): 832 (7), 700 (2), 536 (11), Elemental analysis calcd (%) for; $C_{22}H_{28}N_8Cl_2O_8Ni$: C 39.91, H 4.26, N 16.92; found: C 39.95, H 4.29, N 16.96. Single crystals suitable for X-ray crystallographic analysis were obtained by slow evaporation of a solution of the complex in acetonitrile.

Caution! The perchlorate salts of the compounds are potentially explosive! Only small quantities of these compounds should be prepared and necessary precautions should be taken when they are handled.

2.5. Crystal data collection and structure refinement

Single crystals of complex **2**, suitable for X-ray crystallographic analysis were obtained by slow evaporation of a complex solution in acetonitrile. The diffraction experiments were carried out on a Bruker SMART APEX diffractometer equipped with a CCD area detector. High-quality crystals, suitable for X-ray diffraction were chosen after careful examination under an optical microscope. Intensity data for the crystal was collected using Mo-Kα (k = 0.71073 Å) radiation on a Bruker SMART APEX diffractometer equipped with a CCD area detector at 273 K. The data integration and reduction was processed with SAINT software [43]. An empirical absorption correction was applied to the collected reflections with SADABS [44]. The structure was solved by direct methods using SHELXTL [45] and refined on F^2 by the full-matrix least-squares technique using the SHELXL-97 package [46]. Other non-hydrogen atoms were located in successive difference Fourier syntheses. The final refinement was performed by full-matrix least-squares analysis. Hydrogen atoms attached to the ligand moiety were located from the difference Fourier map. Crystal data and additional details of the data collection and refinement of the structure are presented in Table S1. The selected bond lengths and bond angles are listed in Table 1.

Table 1
Selected bond lengths [Å] and bond angles [°] for complex **2.**

2	
	Bond lengths/Å
Ni(1)-N(1)	2.080(5)
Ni(1)-N(2)	2.166(5)
Ni(1)-N(3)	2.072(5)
Ni(1)-N(5)	2.093(5)
Ni(1)-N(6)	2.159(5)
Ni(1)-N(7)	2.070(5)
	Bond angles [°]
N(2)-Ni(1)-N(7)	175.8(2)
N(3)-Ni(1)-N(7)	101.3(2)
N(6)-Ni(1)-N(7)	81.36(18)
N(2)-Ni(1)-N(6)	96.68(18)
N(3)-Ni(1)-N(6)	174.24(19)
N(1)-Ni(1)-N(7)	97.0(2)
N(1)-Ni(1)-N(6)	92.75(18)
N(1)-Ni(1)-N(2)	79.3(2)
N(1)-Ni(1)-N(5)	167.48(19)
N(1)-Ni(1)-N(3)	91.99(19)
N(5)-Ni(1)-N(7)	91.50(18)
N(5)-Ni(1)-N(6)	79.47(17)
N(5)-Ni(1)-N(2)	91.76(19)
N(5)-Ni(1)-N(3)	95.29(19)
N(2)-Ni(1)-N(3)	81.0(2)

2.6. In vitro antimicrobial activity

Antimicrobial activity was assayed *in vitro* by the disc diffusion susceptibility test according to the recommendations of the National Committee for Clinical Laboratory Standards [47]. Screening for antibacterial activity was performed against common pathogenic bacteria and fungi, including *Pseudomonas aeruginosa* PAO1, *Pseudomonas aeruginosa* PA14, and *Staphylococcus aureus* (ATCC11632), *Salmonella typhi* (MTCC733), *Candida albicans* as well as the marine pathogens, *Vibrio parahaemolyticus* (TFM1) and *Vibrio alginolyticus* (TFM17). Overnight cultures (100 mL) of each pathogen were added to 3 mL of soft Mueller-Hinton agar (MHA; 0.7% w/v agar) and poured onto the surface of MHA plates (15 mL). The complexes were dispensed in sterile distilled water in the concentration of 50, 100, 150, 200 μg/mL and 1 mL were added to 5 mm diameter wells punched with a glass pipette, and plates were incubated at 37 °C up to 72 h. Zones of clear inhibition were measured from the edge of the well [48].

2.7. In vivo antimicrobial acitivity

Antimicrobial activity of complex **1** was determined *in vivo* using brine shrimp (*Artemia franciscana*) against *V. parahaemolyticus* (TFM1) and *V. alginolyticus* (TFM17). In this experiment, the bacterial density 10^4 CFU mL^{-1} was used in all challenge tests with *Artemia* culture. *Artemia* cultures were tested in four groups. Group 1: *Artemia* were maintained with complex **1** and exposed to *Vibrio* spp. Group 2: *Artemia* were maintained with complex **1** only. Group 3: *Artemia* were maintained with *Vibrio* spp. in the absence of complex **1** as positive control.

Table 2
UV–Vis spectral data (λ_{max} in nm; ε in M^{-1} cm^{-1} in parenthesis) of Ni(II) complexes **1** and **2** in acetonitrile at 298 K.

Complex	$^3A_{2g} \rightarrow {}^3T_{1g}(P)$ (ν_3) (nm)		$^3A_{2g} \rightarrow {}^3T_{1g}(F)$ (ν_2) (nm)	$^3A_{2g} \rightarrow {}^3T_{2g}(F)$ (ν_1) (nm)	B′ (cm^{-1})	[b]β (%)
	Found	Calcd[a]				
1	–	320	511 (7)	801 (10)	888	0.82
2	–	344	534 (10)	794 (5)	665	0.62

[a,b]Calculated by solving the quadratic equation and using B as 1080 cm^{-1}.

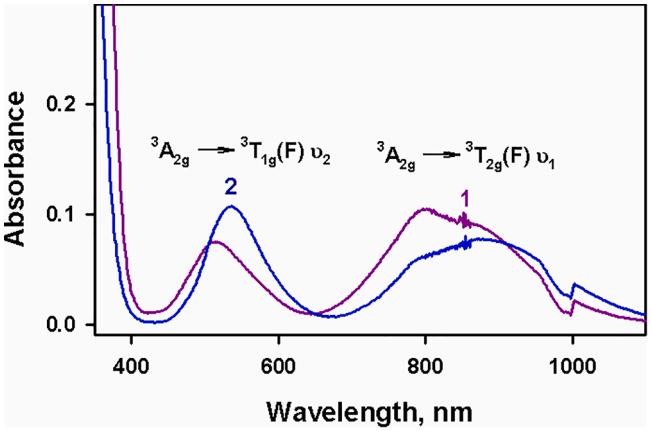

Fig. 1. UV–Visible spectra of the complexes (**1**, and **2**; 1.0 × 10^{-2} M) were recorded in acetonitrile, at 298 K.

Group 4: *Artemia* were maintained alone for control. The mortality rate was monitored every 1 h upto 72 h. Each group has maintained as 20 individuals in 20 mL of sterile seawater and this experiment was done in triplicate. The sterility of this experiment was checked at the end of the challenge; 1 mL of *Artemia* culture was mixed with 9 mL of marine broth in a test tube and incubated for 48 h at 30 °C. The percentage of mortality was calculated by using the formula [(number of mortality/Initial number of survival) × 100)] [49].

3. Results and discussion

3.1. Synthesis and characterization of the N3 ligands and nickel(II) complexes

The tridentate N3 ligands L1 and L2 were synthesized according to the known procedures [38–42], which involves Schiff base condensation of the corresponding aldehydes with amines followed by reduction with sodium borohydride. The nickel(II) complexes **1** and **2** were prepared by adding two equivalents of the ligand to an aqueous methanolic solution of $Ni(ClO_4)_2{\cdot}6H_2O$. Both the complexes are formulated as $[Ni(L)_2](ClO_4)_2$ based on UV–Vis, IR, paramagnetic NMR spectroscopic techniques, ESI-MS and single-crystal X-ray structure analysis. In fact, complex **1**, has been reported previously in the literature [39]. Single-crystal x-ray structure determination reveals that complex **2** also possesses distorted octahedral coordination geometry with two facial tridentate ligand coordination as similar to complex **1** [39]. The thermal behaviour of complexes **1** and **2** was examined using TGA and DSC and they were found to be thermally stable up to 201 ℃ and 217 ℃, respectively. Both the complexes are expected to show promising antimicrobial activity against different pathogens (Gram-negative and Gram-positive) due to the coordination of metal ion to heterocyclic ring nitrogen.

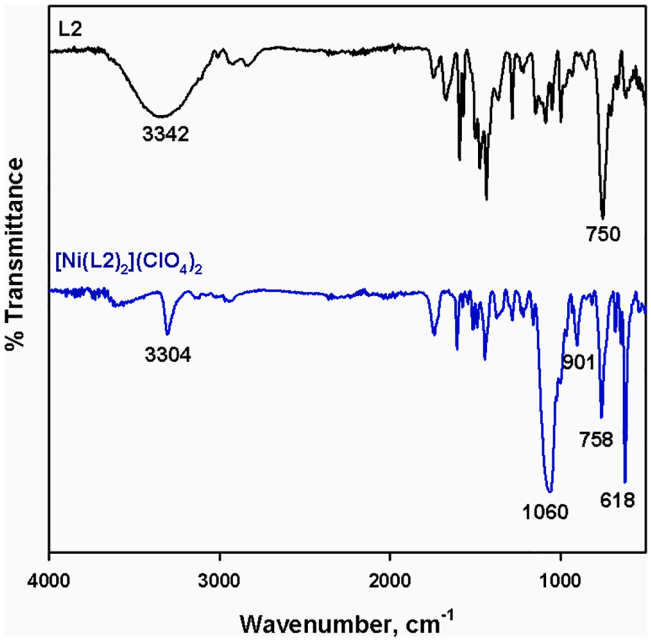

Fig. 2. ATR IR spectra of the ligand L2 (top) and $[Ni(L2)_2](ClO_4)_2$ **2** (bottom).

3.2. Electronic absorption spectral properties

Although complex **1** has been reported previously, we also attempted to characterize it with a variety of spectroscopic techniques to have a better comparison with **2**. In the following section, we have discussed the results.

The electronic absorption spectra of complexes **1** and **2** were recorded in acetonitrile, at 298 K and the data are summarized in Table 2. The typical spectra are presented in Fig. 1. Both the complexes exhibit two broad absorption bands in the range of λ(nm), 511–534 and λ(nm), 801–794. The peaks are assigned to various transitions that are usually observed in typical Ni(II) complexes, with the help of the Tanabe-Sugano diagram. UV–Vis spectra of complex **1** perfectly matches with the reported wavelengths and it reveals that we also isolated the same octahedral coordinated complex **1** [39]. The lowest energy transition is the $^3A_{2g}(F) \rightarrow {}^3T_{2g}(F)$ (ν_1), which gives rise to the broad absorption bands in the range of 801–794 nm, while the $^3A_{2g}(F) \rightarrow {}^3T_{1g}(F)$ (ν_2) transition gives rise to the bands in the range of 511–534 nm. Using ν_1 and ν_2 transitions, we have calculated the $^3A_{2g}(F) \rightarrow {}^3T_{1g}(P)$ (ν_3) transition for both the complexes (**1**, 320: **2**, 344 nm), however, it was not observed experimentally and it might be overlapped with the ligand-based high energy transitions. This data is in good accordance with that of the previously reported octahedral Ni(II) complexes [39,50–55]. The ν_1 band position depends on the donor atom type; thus, when the pyridylmethyl arm in complex **1** is replaced an imidazolylmethyl arm to obtain complex **2**, the ν_1 band is shifted slightly to higher energy because of the strongly σ-bonding imidazole donor atom as expected based on the literature [50–55]. The metal–ligand covalency parameter β was calculated for both complexes (**1**, 0.82; **2**, 0.62) [54]. The higher β value for complex **1** can be attributed to the strong π-back donating ability of the pyridine N atoms, as has been observed previously in other reported complexes [39,50–55]. These observations confirm that the Ni(II) complexes **1** and **2** have octahedral geometry in solution. In addition, we have recorded the paramagnetic ^{1}H NMR for both complexes and the peaks were observed in the more downfield region, which again confirms the octahedral coordination geometry in solution (Figs. S5, and S6) [39].

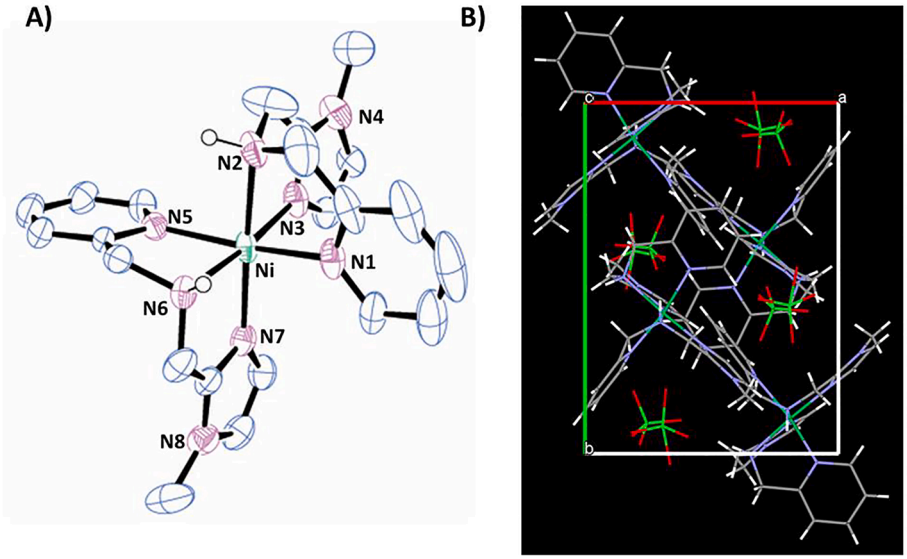

Fig. 3. (A) ORTEP diagram of $[Ni(L2)_2]^{2+}$ **2** showings 50% probability thermal ellipsoids and the labelling scheme for selected atoms. All the hydrogen atoms are omitted for clarity. (B) A crystal packing diagram of **2**, viewed along the c axis.

3.3. Infrared Spectroscopy

The infrared (IR) spectra of the ligands and complexes were recorded by employing the Attenuated Total Reflection (ATR) technique. Both the ligands exhibit the principal peaks in the range of 3333 – 3342 cm^{-1} and 748 – 750 cm^{-1}, that have been assigned to the N—H and C—N stretching frequencies, respectively (Figs. 2 and S2). The peak at 3333 cm^{-1} of Ligand L1 and 3342 cm^{-1} of Ligand L2 is very broad, owing to hydrogen bonding between the N—H and H_2O. These peaks were observed to be slightly shifted in the corresponding complexes **1** and **2**. The decrease in N—H stretching frequency (**1**, 3282 from 3333 cm^{-1}; **2**, 3304 from 3342 cm^{-1}) and its sharp nature indicates complex formation without hydrogen bonding and the increase in C—N stretching frequency to (**1**, 753 from 748 cm^{-1}; **2**, 758 from 750 cm^{-1}) is explained by the attraction of the aromatic ring electrons toward nitrogen, due to a deficiency in its electron density upon coordination to the nickel(II) center. Also, the broad intense peak around for **1**, 1052 cm^{-1}; **2**, 1060 cm^{-1}, sharp intense peak at 618 nm and the weaker absorption peak around the range (**1**, 910 cm^{-1}; **2**, 901 cm^{-1}) indicates the presence of the uncoordinated ClO_4^- ions [56].

3.4. Description of the structure of $[Ni(L2)_2](ClO_4)_2$ 2 and comparison with $[Ni(L1)_2](ClO_4)_2$ 1

The molecular structure of complex cation of $[Ni(L2)_2](ClO_4)_2$ **2** is shown in Fig. 3A, together with the atom numbering scheme and the principal bond length and bond angles are collected in Table 1. The complex cation of **2** possesses a NiN_6 coordination sphere with distorted octahedral coordination geometry where two pyridine of the **1** is replaced by two imidazole groups. Both the ligands are facially coordinated with the two coordinating secondary amino- and two imidazolyl groups being *cis* to each other. The Ni–N_{py} (2.080, 2.093 Å), Ni–N_{amine} (2.159, 2.166 Å) and Ni–N_{im} (2.070, 2.072 Å) bond distances fall in the ranges observed for the previously reported nickel(II) complexes (Ni–N_{im}, 1.999–2.134 Å) [50,54,55,57,58]. The Ni–$N3_{im}$ bond length (2.072 Å) is shorter than the Ni–N_{py} bond lengths (2.080 Å) as the coordination of imidazole is stronger than that of pyridine donor [p*K*a (BH^+): pyridine, 5.2; imidazole, 7.01]. The Ni–N_{py} (2.080, 2.093 Å) and Ni-N_{im}(2.070, 2.072 Å) bond lengths are shorter than the Ni–N_{amine} bond lengths (2.159, 2.116 Å) due to sp^2 and sp^3 hybridization of pyridyl, imidazolyl and amine nitrogen donors, respectively.

The N–Ni–N (79.3(2)°–101.3(2)°) and N–Ni–N (167.48(19)°– 175.8 (2)°) bond angles deviate from the ideal octahedral angles of 90° and 180°, respectively, revealing that there is significant distortion in octahedral coordination geometry around Ni(II). A crystalline arrangement of complex **2** viewed along the *c* axis is illustrated in Fig. 3B. It is noteworthy that the oxygen atoms in one of the ClO_4^- anions were found

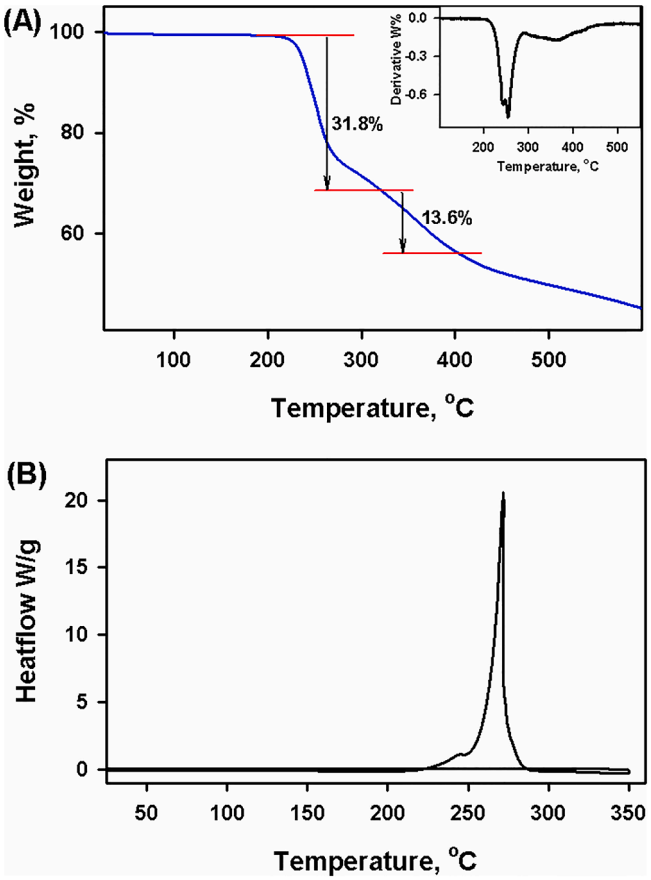

Fig. 4. (A) Thermogravimetric curve for **2**, Derivative (weight%) curve for **2**, under inert N_2 atmosphere up to 600℃ (Inset) (B) DSC curve for **2** under inert N_2 atmosphere up to 350℃.

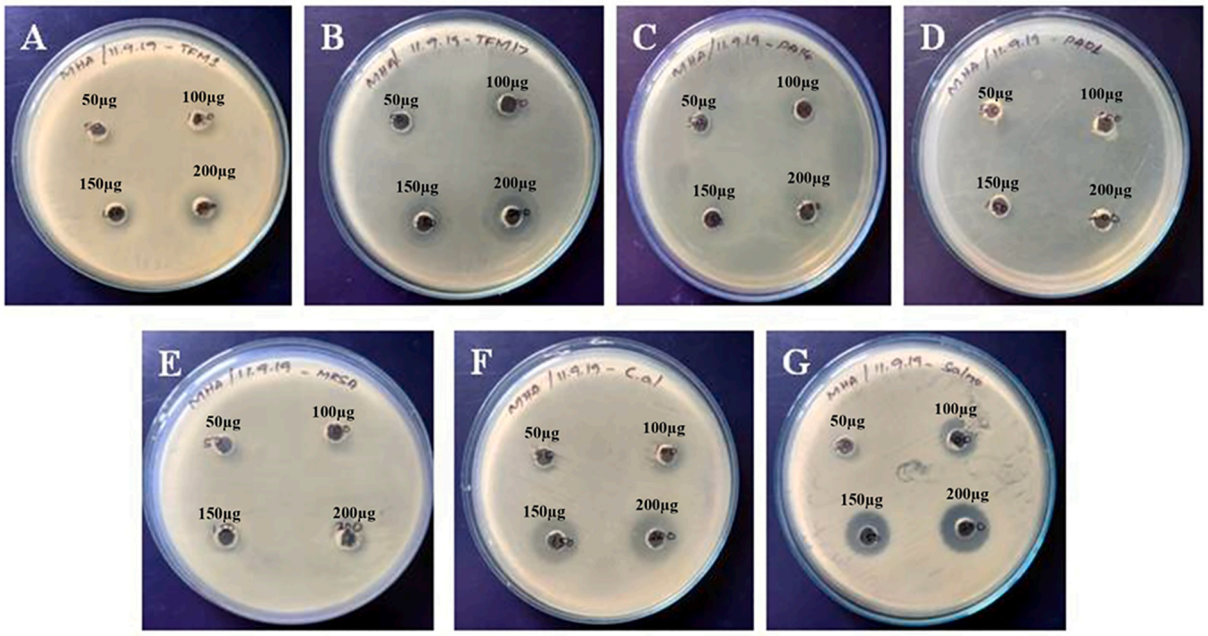

Fig. 5. *In vitro* antimicrobial studies of complex **1 with (A)** ***Vibrio parahaemolyticus,*** **(B)** ***Vibrio alginolyticus,*** **(C)** ***Pseudomonas aeruginosa PA14,*** **(D)** ***Pseudomonas aeruginosa PAO1,*** **(E)** ***Staphylococcus aureus (MRSA),*** **(F)** ***Candida albicans,*** **(G)** ***Salmonella typhi.***

to exhibit multiple equilibria.

The complex cation of **1** possesses a NiN_6 coordination sphere with a distorted octahedral coordination geometry constituted by four pyridyl and two secondary amine nitrogen atoms from two tridentate ligands [39]. The ligand L1 is facially coordinated, conferring a *cis* coordination geometry on Ni(II). The Ni–N_{py} bond length (2.102(5) Å) is shorter than the Ni–N_{amine} bond lengths (2.106(4), 2.113(5) Å) due to sp^2 and sp^3 hybridization of pyridyl and amine nitrogen donors, respectively [39]. The N–Ni–N (80.77(17)°–104.21(16)°) and N–Ni–N (167.56(14)°–173.93(19)°) bond angles deviate from the ideal octahedral angles of 90° and 180°, respectively, revealing that the octahedral coordination geometry around Ni(II) is significantly distorted [39].

3.5. Thermal studies (TGA/DSC)

The thermal analysis of complexes $[Ni(L1)_2](ClO_4)_2$ **1** and $[Ni(L2)_2](ClO_4)_2$ **2** was carried out under an inert atmosphere by heating at a rate of 5 °C. According to the TG curve, both the nickel(II) complexes are stable upto 200 °C. Complex **1** loses weight in two steps as shown in Fig. S7A. The first step spans between 201 °C and 278 °C, which corresponds to 1.4%. The second thermolytic step starts at 206 °C and ends at 414 °C with 48% weight loss and it can be due to the loss of four pyridine molecules (Fig. S7A). The sharp exothermic peak at 272 °C in the DSC curve of **1** gives the total heat effect of the process (Fig. S7B). For complex **2,** the first step spans between 217 °C and 328 °C, corresponds to a weightloss of 31.8% and can be due to the loss of two perchlorate molecules (Fig. 4A). The second thermolytic step starts at 328 °C and ends at 427 °C with 13.6% weight loss. The total heat effect of the above process is observed as a sharp exothermic peak at 272 °C in the DSC curve of **1** and 302 °C in the DSC curve of **2** shown in Fig. 4B. The derivative (W%) curve in Fig. S7A (Inset) and Fig. 4A (Inset) gives the exact temperature value in the form of the endothermic peak for complex **1** and **2** respectively.

3.6. Antimicrobial activity

Complexes **1** and **2** were tested for the *in vitro* antimicrobial activity by well diffusion method against Gram-negative bacteria: *Pseudomonas aeruginosa* (PAO1), *Pseudomonas aeruginosa* (PA14), and *Salmonella typhi* (MTCC733), Gram-negative marine pathogens: *Vibrio parahaemolyticus* (TFM1) and *Vibrio alginolyticus* (TFM17), Gram-positive bacterium *Staphylococcus aureus* (ATCC11632), as well as fungi, *Candida albicans*. In the present study, both the complexes exhibited antibacterial activity against both Gram-positive and Gram-negative pathogens (Fig. 5 and Fig. S8). The molecules that show wide activity against bacteria and fungi will have a broader application. Complex **1** displayed activity against all the pathogens tested except for *P. aeruginosa*. Whereas, complex **2** displayed activity against *S. typhi, S. aureus* and *C. albicans*. Both the complexes inhibited the growth of *C. albicans* while none of the complexes inhibited the growth of *P. aeruginosa*. As the concentration increases, there was a significant increase in antimicrobial activity for both the complexes. Table 3 shows the MIC of both the complexes against different pathogens tested. The antifungal activity of complex **1** and **2** is more pronounced than their antibacterial activity. Complex **1** inhibited the growth of *C. albicans* and has a better MIC when compared to the reported nickel complexes of **C** and **E** (Scheme 1). However, complex **2** has a reasonable MIC against *C. albicans* when compared with these complexes [20,22].

Table 3
The minimal inhibitory concentration of complexes **1** and **2.**

S. No.	Organisms	MIC of **1** (µg/mL)	MIC of **2** (µg/mL)
1	*V. parahaemolyticus* (TFM 1)	125 ± 13	–
2	*V. Alginolyticus* (TFM 17)	90 ± 7	–
3	*Staphylococcus aureus* (ATCC11632)	140 ± 12	85 ± 9
4	*Salmonella typhi* (MTCC733)	80 ± 9	130 ± 10
5	*Candida albicans*	20 ± 5	110 ± 7

One of the most common modes of action of antimicrobials is cell membrane disruption and here the increased lipophilicity of the central metal atom by chelation would facilitate the penetration through the lipid bilayer of cell membrane [20,22]. The relation between the ligand system and antimicrobial activity is evident from the MIC value (Table 3), which increased in the case of *S.typhi* and *C.albicans* and decreased for *S. aureus* when one of the pyridyl donor in **1** was replaced

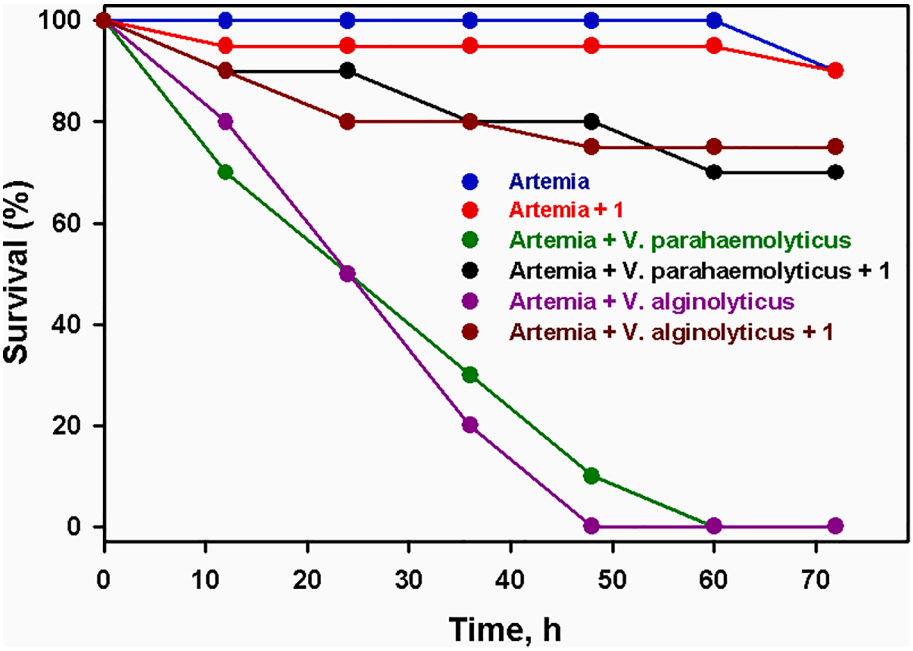

Fig. 6. Survival graphs of TFM1 and TFM17 showing the rescued survival of brine shrimp larvae supplemented with 150 μg $mL^{-1}$of **1**.

by imidazolyl donor to obtain **2**. Further, imidazole interacts with receptors and enzymes of microbes through different interactions such as inhibiting NO dioxygenase (NOD) function by coordinating to flavohemoglobin (flavoHb) which induce antimicrobial activity and particularly the fungicidal effect is correlated with the inhibition of the dimorphic transition, ergosterol biosynthesis and mitochondrial activity [59–61].

3.7. Toxicity and therapeutic potential of complex 1 to brine shrimp larvae against Vibrio spp.

Here, the ability of complex **1** to protect the model animal gnotobiotic *Artemia franciscana* from pathogenic *Vibrio* isolates TFM1 and TFM17 was investigated. Besides, toxicity of complex **1** on *Artemia* also examined. Complex **1** showed no toxicity on *Artemia* at 20 μg mL^{-1} and 150 μg mL^{-1}. *Vibrio* spp. TFM1 and TFM17 caused 80–100% and 90–100% mortality respectively in *Artemia* in the absence of complex **1**.

Complex **1** radically improved the survival of *Artemia* up to 75% (against TFM1) and 85% (against TFM17) (Fig. 6). For *in vivo* challenges, the brine shrimp larvae were used as a bio-monitor animal model system to detect the impact of complex **1** against *Vibrio* infection. Due to the antimicrobial activity of complex **1** against *Vibrio* spp, the survival rate of brine shrimp larvae was not affected in the presence of complex **1**. Moreover, complex **1** also protected the larvae from the colonization of *Vibrio* pathogens in their gut. These initial findings would be helpful to guide the future research in finding the most optimal application in the field of aquaculture to combat against multi-drug resistant pathogens.

4. Conclusion

The tridentate (N3) ligands bis(pyridin-2-ylmethyl)amine (L1) and 1-(1-methyl-1*H*-imidazol-2-yl)-*N*-(pyridin-2-ylmethyl)methanamine (L2) and their corresponding Ni(II) complexes have been synthesized and characterized by UV–Visible, IR, paramagnetic ^{1}H NMR spectroscopic techniques, mass spectrometry and single-crystal X-ray and thermal analysis. The crystal structure of complex **2** has been found to possess a distorted octahedral geometry by the facial coordination of two tridentate N3 ligands to nickel(II) center as similar to the complex **1** [39]. UV–Visible spectral pattern which is similar to that of previously reported Ni(II) complexes along with the paramagnetic ^{1}H NMR spectra helps in confirming the octahedral geometry of complexes **1** and **2** in solution. The higher β value for complex **1** is attributed to the strong π-back donating ability than complex **2** and, it is in accordance with the literature [39]. Further, degradation of the complexes occurs in consecutive reactions, which is determined by thermal analysis. Overall, the present study concluded that both complexes **1** and **2** have antibiotic activity against the tested pathogens. The antifungal activity of complex **1** is more pronounced. *In vivo* studies showed that complex **1** is effective in preventing *Vibrio* infection in brine shrimp. This could ultimately improve the aquaculture productivity by preventing *Vibrio* infections in *Artemia*.

CRediT authorship contribution statement

Athulya Das: Data curation, Formal analysis, Investigation, Methodology, Project administration, Resources, Software, Writing – original draft, Writing – review & editing. **Anjana Rajeev:** Data curation, Investigation, Methodology, Project administration, Resources, Software. **Sarmistha Bhunia:** Data curation, Investigation, Methodology, Project administration, Resources, Software. **Manivel Arunkumar:** Data curation, Investigation, Methodology, Project administration, Resources, Software. **Nithya Chari:** Formal analysis, Investigation, Methodology, Project administration, Resources, Software, Supervision, Validation, Visualization, Writing – original draft, Writing – review & editing. **Muniyandi Sankaralingam:** Conceptualization, Formal analysis, Funding acquisition, Investigation, Methodology, Project administration, Resources, Software, Supervision, Validation, Visualization, Writing – original draft, Writing – review & editing.

Declaration of Competing Interest

The authors declare that they have no known competing financial interests or personal relationships that could have appeared to influence the work reported in this paper.

Acknowledgments

AD and AR acknowledge the DST-Inspire (IF-170136), and UGC-JRF

for their fellowship, respectively. MS sincerely acknowledges the Department of Science and Technology for the award of the DST-Inspire Faculty research grant (IFA-17-CH286) and also the National Institute of Technology Calicut for the Faculty Research Grant. Also, we sincerely, acknowledge Prof. Abhishek Dey, School of Chemical Sciences, Indian Association for the Cultivation of Sciences (IACS), Kolkata for helping us in collecting the ESI-MS and NMR data.

Appendix A. Supplementary data

Supplementary data to this article can be found online at https://doi.org/10.1016/j.ica.2021.120515.

References

[1] D.E. Bloom, D. Cadaratte, Front. Immunol. 10 (2019). Article 00549.
[2] WHO, Antiocrobial resistance. https://www.who.int/news-room/fact-sheets/detail/antimicrobial-resistance, accessed 18.11.2020.
[3] SGanesh Kumar, C. Adithan, B.N. Harish, G. Roy, A. Malini, S. Sujatha, Antimicrobial resistance in India: a review, J. Nat. Sci. Biol. Med. 4 (2) (2013) 286, https://doi.org/10.4103/0976-9668.116970.
[4] J. Davies, D. Davies, Microbiol. Mol. Biol. Rev. 73 (2010) 417–433.
[5] R.J.P. Williams, R. Inst, Chem. Rev. 1 (1968) 13–38.
[6] G.B. Bagihalli, P.G. Avaji, P.S. Badami, S.A. Patil, J. Coord. Chem. 61 (2008) 2793–2806.
[7] A.H. Maikshete, S.A. Sarsamkar, S.A. Deodware, V.N. Kamble, M.R. Asabe, Inorg. Chem. Commun. 14 (2011) 618–621.
[8] Z. Afrasiabi, E. Sinn, J. Chen, Y. Ma, A.L. Rheingold, L.N. Zakharov, N. Rath, S. Pandhye, Inorg. Chim. Acta. 357 (2004) 271–278.
[9] S.S. Harmalkar, R.J. Butcher, V.V. Gobre, S.K. Gaonkar, L.R. D'Souza, M. Sankaralingam, I. Furtado, S.N. Dhuri, Inorg. Chim. Acta. 498 (2019) 119020.
[10] K. Singh, Y. Kumar, P. Puri, M. Kumar, C. Sharma, Eur. J. Med. Chem. 52 (2012) 313–321.
[11] P. Tharmaraj, D. Kodimunthiri, C.D. Sheela, C.S.S. Priya, J. Coord. Chem. 62 (2009) 2220–2228.
[12] A.A. El-Sherif, Inorg. Chim. Acta 362 (2009) 4991–5000.
[13] N. Raman, V. Muthuraj, S. Ravichandran, A. Kulandaisami, Proc. Indian, Acad. Sci. 115 (2003) 161–167.
[14] Z.H. Chohan, M.A. Farooq, Synth. React. Inorg. Met. Org. Chem. 31 (2001) 1853–1871.
[15] N.E. Dixon, C. Gazzola, R.L. Blakeley, B. Zerner, J. Am. Chem. Soc. 97 (1975) 4131–4133.
[16] E.M. Jouad, G. Larcher, M. Allain, A. Riou, G.M. Bouet, M.A. Khan, X.D. Thanh, J. Inorg. Biochem. 86 (2001) 565–571.
[17] N.C. Kasuga, A. Ohashi, C. Kouma, J. Uesugi, M. Oda, K. Nomiya, Chem. Lett. (1997) 609–610.
[18] N.C. Kasuga, K. Sekino, C. Koumo, N. Shimada, M. Ishikawa, K. Nomiya, J. Inorg. Biochem. 84 (2001) 55–65.
[19] M. Alexiou, I. Tsivikas, C.M. Samara, A.A. Pantazaki, P. Trikalitis, N. Lalioti, D. A. Kyriakidis, D.P. Kessissoglou, J. Inorg. Biochem. 93 (2003) 256–264.
[20] R. Kurtaran, L.T. Yildirim, A.D. Azaz, H. Namil, O. Atakol, J. Inorg. Biochem. 99 (2005) 1937–1944.
[21] K.C. Skyrianou, E.K. Efthimiadou, V. Psycharis, A. Terzis, D.P. Kessissoglou, G. Psomas, J. Inorg. Biochem. 103 (2009) 1617–1625.
[22] P. Raj, A. Singh, A. Singh, N. Singh, A.C.S. Sustain, Chem. Eng. 5 (2017) 6070–6080.
[23] S.D. Oladipo, B. Omondi, C. Mocktar, Polyhedron 170 (2019) 712–722.
[24] M.S. Saini, A. Kumar, J. Dwivedi, R. Singh, Int. J. Pharm. Sci. Res. 4 (2013) 66–77.
[25] D. Lednicer, L.A. Mitscher, Organic Chemistry of Drug Synthesis, Wiley Inter science publication, 1984.
[26] A.P. Taylor, R.P. Robinson, Y.M. Fobian, D.C. Blakemore, Lyn H. Jones, O. Fadeyi, Org. Biomol. Chem. 14 (2016) 6611–6637.
[27] R.D. Taylor, M. MacCoss, A.D.G. Lawson, J. Med. Chem. 57 (2014) 5845–5859.
[28] G.V.M. Sharma, A. Ramesh, A. Singh, G. Sarikanth, V. Jayaram, D. Duscharla, J. Ho Jun, R. Ummanni, Med. Chem. Commun. 5 (2014) 1751–1760.
[29] A. Khalafi-Nezhad, M.N.S. Rad, H. Mohabatkar, Z. Asrari, B. Hemmateenejad, Bioorg. Med. Chem. 13 (2005) 1931–1938.
[30] W.H. Beggs, F.A. Andrews, G.A. Sarosi, Life. Sci. 28 (1981) 111–118.
[31] T.-C. Chien, S.S. Saluja, J.C. Drach, L.B. Townsend, J. Med. Chem. 47 (2004) 5743–5752.
[32] Y.-L. Fan, X.-H. Jin, Z.-P. Huang, H.-F. Yu, Z.-G. Zeng, T. Gao, L.-S. Feng, Eur. J. Med. Chem. 150 (2018) 347–365.
[33] P. Kiuru, J. Yil-Kauhaluoma, in: Heterocycles in Natural Product Synthesis, Wiley-VCH, Weinheim, Germany, 2011, p. 267.
[34] Y.W. Jo, W.B. Im, J.K. Rhee, M.J. Shim, W.B. Kim, E.C. Choi, Bioorg. Med. Chem. 12 (2004) 5909–5915.
[35] K.C. Nicolaou, R. Scarpelli, B. Bollbuck, B. Werschkun, M.M.A. Pereira, M. Wartmann, K.-H. Altmann, D. Zaharevitz, R. Gussio, P. Giannakakou, Chem. Biol. 7 (2000) 593–599.
[36] J. Bernstein, B. Stearns, M. Dexter, W.A. Lott, J. Am. Chem. Soc. 69 (1947) 1147–1150.
[37] M.H. Helal, S.A. El-Awdan, M.A. Salem, T.A. Abd-elaziza, Y.A. Mohamed, A.A. El-Sherif, G.A.M. Mohamed, Spectrochim. Acta A. 135 (2015) 764–773.
[38] M. Sankaralingam, M. Palaniandavar, Polyhedron 67 (2014) 171–180.
[39] M. Velusamy, M. Palaniandavar, K.R.J. Thomas, Polyhedron 17 (1998) 2179–2186.
[40] T. Dhanalakshmi, E. Suresh, M. Palaniandavar, Dalton Trans. (2009) 8317–8328.
[41] K. Sundaravel, E. Suresh, M. Palaniandavar, Inorg. Chim. Acta 363 (2010) 2768–2777.
[42] M. Velusamy, R. Mayilmurugan, M. Palaniandavar, J. Inorg. Biochem. 99 (2005) 1032–1042.
[43] G.M. Sheldrick, SAINT 5.1 ed., Siemens Industrial Automation Inc., Madison, WI, 1995.
[44] SADABS Empirical Absorption Correction Program, University of Göttingen, Göttingen, Germany, 1997.
[45] G.M. Sheldrick, SHELXTL Reference Manual: Version 5.1, Bruker AXS, Madison, WI, 1997.
[46] G.M. Sheldrick, SHELXL-97: Program for Crystal Structure Refinement, University of Göttingen, Göttingen, Germany, 1997.
[47] NCCLS Methods for Dilution Antimicrobial Susceptibility Tests for Bacteria that Grow Aerobically. 2000. Document M7-A5, 5th ed. Wayne, PA: National Committee for Clinical Laboratory Standards.
[48] J. Nissimov, E. Rosenberg, C.B. Munn, FEMS Microbiol. Lett. 292 (2009) 210–215.
[49] I.A.S.V. Packiavathy, P. Sasikumar, S.K. Pandian, A.V. Ravi, Appl. Microbiol. Biotechnol. 23 (2013) 10177–10187.
[50] M. Sankaralingam, P. Vadivelu, M. Palaniandavar, Dalton Trans. 46 (2017) 7181–7193.
[51] M. Sankaralingam, P. Vadivelu, E. Suresh, M. Palaniandavar, Inorg. Chim. Acta 407 (2013) 98–107.
[52] M. Sankaralingam, M. Balamurugan, M. Palaniandavar, P. Vadivelu, C.H. Suresh, Chem. Eur. J. 20 (2014) 11346–11361.
[53] A.B.P. Lever, J. Chem. Educ. 45 (1968) 711–712.
[54] M. Balamurugan, R. Mayilmurugan, E. Suresh, M. Palaniandavar, Dalton Trans. 40 (2011) 9413–9424.
[55] M. Sankaralingam, M. Balamurugan, M. Palaniandavar, Coord. Chem. Rev. 403 (2020) 213085.
[56] A.E. Wickenden, R.A. Krause, Inorg. Chem. 4 (1965) 404–407.
[57] Y. An, X.-F. Li, Y.-L. Zhang, Y.-S. Yin, J.-J. Sun, S.-F. Tong, H. Yang, S.-P. Yang, Inorg. Chem. Commun. 38 (2013) 139–142.
[58] D.M. Gil, H. Osiry, A. Rodriguez, A.A. Lemus-Santana, R.E. Carbonio, E. Reguera, Eur. J. Inorg. Chem. 2016 (2016) 1690–1696.
[59] R.A. Helmick, A.E. Fletcher, A.M. Gardner, C.R. Gessner, A.N. Hvitved, M. C. Gustin, P.R. Gardner, Antimicrob. Agents. Chemother. 49 (2005) 1837–1843.
[60] I.J. Sud, D.S. Feingold, J. Investig. Dermatol. 76 (1981) 438–441.
[61] E. Pinto, H. Neves, K. Hrimpeng, A.-F. Silva, A. Begouin, G. Lopes, M.-J.R. P. Queiroz, Mini. Rev. Med. Chem. 14 (2014) 941–952.